Force–Displacement Characteristics of Helical Soil Nail under Monotonic Pullout Loading: Experimental and Theoretical Study

Pankaj Sharma[1] · Saurabh Rawat[1] · Ashok Kumar Gupta[1]

Abstract This study investigates the shear stress–displacement behavior of helical soil nails (HSN) under different overburden pressure and monotonic pullout loading. Two types of individual HSN (ribbed solid and hollow plain) and a group of nine ribbed solid shafts HSN installed with uniform spacing are experimentally investigated. The study also examines vertical stresses and axial stresses developed along with HSNs. Further, theoretical modeling of the obtained experimental stress–displacement behavior has also been carried out. The results depict mobilization of nonlinear stresses under monotonic pullout for both individual and group HSN. The stress–displacement behavior is vividly marked by a pre-peak and post-peak stage. Higher shear stress mobilization is found for solid HSN as compared to hollow ones. A close agreement with a low coefficient of variance between measured and predicted values for overburden pressure between 5 and 50 kPa depicts the efficacy of the developed theoretical model. The results of axial strain for both shaft types HSN reveal strain softening during post-peak, which diminishes in case of group behavior. It is concluded that truncated cone rupture failure during group behavior significantly governs the stress–displacement response majorly by bearing than interface shearing resistance of soil plugging in hollow shafts.

✉ Saurabh Rawat
  saurabh.rawat@juit.ac.in

  Pankaj Sharma
  iisc0700ps@gmail.com

  Ashok Kumar Gupta
  ashok.gupta@juit.ac.in

[1] Department of Civil Engineering, Jaypee University of Information Technology, Solan, H.P 173234, India

Introduction

Soil nailing has proved a time- and cost-efficient ground improvement technique since its inception in the late twentieth century. Since then, the soil nailing technique is continuously under up-gradation with its usage extending from tunneling, vertical excavation to highway and railway widening projects and eventually for slope and fill stabilization [1, 2]. The top-down construction procedure involves drilling of a borehole, placement of steel, GFRP [3] or bamboo [4] inclusion, and subsequent grouting. During the installation of traditional soil nails, problems such as in situ soil disturbances due to drilling, inadequate grout distribution due to faulty drilling, and production of significantly large soil spoils are often encountered. In addition, restriction of drilling in cohesionless soils leading to borehole collapse and soil nailing below groundwater table due to its susceptibility for corrosion and alteration of grout–water ratio are also associated problems of traditional nailing technique. Because of these lacunae, many recent researchers [5–8] have attempted to incorporate the concept of helical piles and anchors to overcome the installation difficulties and facilitate nailing below saturated soil conditions. This kind of soil nail is termed as helical soil nail.

The concept of soil–structure interaction as listed by Mitsch and Clemence [9] was primarily governed by interface pile/anchor shaft–soil frictional resistance and bearing resistance offered by the helical plates attached along the pile/anchor shaft. Helical soil nails (HSNs) are

generally used to mobilize higher pullout strength due to the presence of helices against pullout load, and overturning moments. Owing to the advantages of quick installation, least disturbance, and instantaneous loading potential, their extent of use has prolonged beyond the conventional applications to hydraulic structures, tunnels, and unstable slopes, excavations, and embankments [10, 11]. Helical nail is considered a modern substitute for traditional soil nail applications. HSN is installed under the action of torque and offers bearing capacity from the helix blade affixed to the nail shaft. As per Perko [10] for helical plates spaced at a distance of 3 times the helix diameter (D_h), helical plate bearing predominates the behavior of helical elements both during compressive and tensile loading. To further enhance the soil–shaft interaction, Han et al. [12] suggested the use of an open-ended pipe pile for incorporating the soil plug phenomena is providing additional internal shaft friction and annulus bearing during pile driving. Using a similar approach Sharma et al. [13, 14] evaluated the behavior of hollow helical nails to assess the advantage of soil plugging during the pullout. It was observed that the internal frictional resistance contributes about 11.5% of total shaft friction. Moreover, the remaining resistance was found to be attained mainly by the helical bearing instead of outer shaft friction.

As per FHWA [1], the internal stability of a soil-nailed structure is largely dependent on the pullout force of the soil nail. The pullout failure mode is defined as the failure occurring at the soil–grout interface due to the movement of active soil wedge under surcharge loading. The mobilized shear stress at the soil–grout interface is inadequate due to weak bond strength or smaller pullout nail length. The review of the literature [15–18] revealed that mobilized pullout resistance is governed by various parameters, such as in situ soil conditions, soil saturation, soil nail configuration and geometry, surcharge pressure, overburden pressure, installation method, grouting pressure, and roughness of grout–nail and soil–grout interface. Extensive laboratory and field studies have been carried out by researchers on traditional soil nails for the evaluation of pullout capacity and its parametric variation [19–23]. However, in the context of helical soil nails, pullout failure is related to the load which causes a continuous pullout movement (creep) of helical soil nails. This pullout load may not necessarily be the maximum pullout load [11].

Moreover, the literature presently available regarding pullout investigation of helical soil nails through laboratory testing or numerical modeling primarily focuses on interpreting the pullout response with increasing surcharge, the effect of shaft diameter, helix diameter, number of helices, and helical spacing [7, 8, 24–30]. Tokhi et al. [25] found that the pullout behavior of helical soil nails is comparable to traditional nails up to 130 kPa depicting good agreement

in terms of apparent coefficient of friction also. However, the evaluated apparent friction was conservative as the contribution of helical bearing was neglected. A similar experimental study conducted by Sharma et al. [23] also observed an increase in pullout response of helical soil nails with progressive displacement up to a peak pullout load and thereafter becoming constant. To further comprehend the pullout response, Rawat et al. [27] through three-dimensional finite element modeling recorded strain-softening phenomenon with an increasing number of helices during the pullout.

Among the limited helical soil nail pullout studies prevalent, lacunae for extensive investigation of stress–strain characteristics exists for clearly understanding the mechanism occurring during helical nail pullout. Moreover, to closely model the actual field conditions, stress–strain condition mobilized during group action of helical nails becomes essential. The comprehension of developed and mobilized pullout stress–strain will enable decipher the progressive failure occurring at the soil–nail interface.

Therefore, the present study aims at investigating the stress–strain condition mobilized at the helical soil nail (HSN) under a monotonic pullout loading. The study is conducted on a single helical nail and a group of nine helical nails arranged in a uniform configuration. The parametric study involves studying the stress–strain variation with increasing surcharge pressure and different circular shaft type [ribbed solid (RS) and plain hollow (PH)]. Furthermore, the assessment of axial strains under progressive horizontal displacement developed along HSN length is also studied. Finally, analytical analysis of the observed stress–stain behavior is carried out and compared with the experimental results.

Mechanism of Helical Nail Pullout

Helical soil nails differ from helical anchors based on the fact that anchors are pre-tensioned elements against nails that require movement for mobilization of shearing resistance [28]. During failure as the helical soil-nailed structure undergoes lateral movement, the slip surface propagating across the nails forms two distinct soil wedges. The wedge enclosed within the slip surface and facing constitute the active surface and the passive wedge is formed beyond the slip surface. The helical nail length extending in the passive wedge determines the pullout resistance of the helical nail. Moreover, as per field practices, the adopted helical plate spacing is $3D_h$ which facilitates the development of individual bearing failure mechanism during pullout [8, 11, 29]. Thus, for individual helical nails under pullout loading (Fig. 1), it can be seen that pullout resistance (P_R) of the helical element is
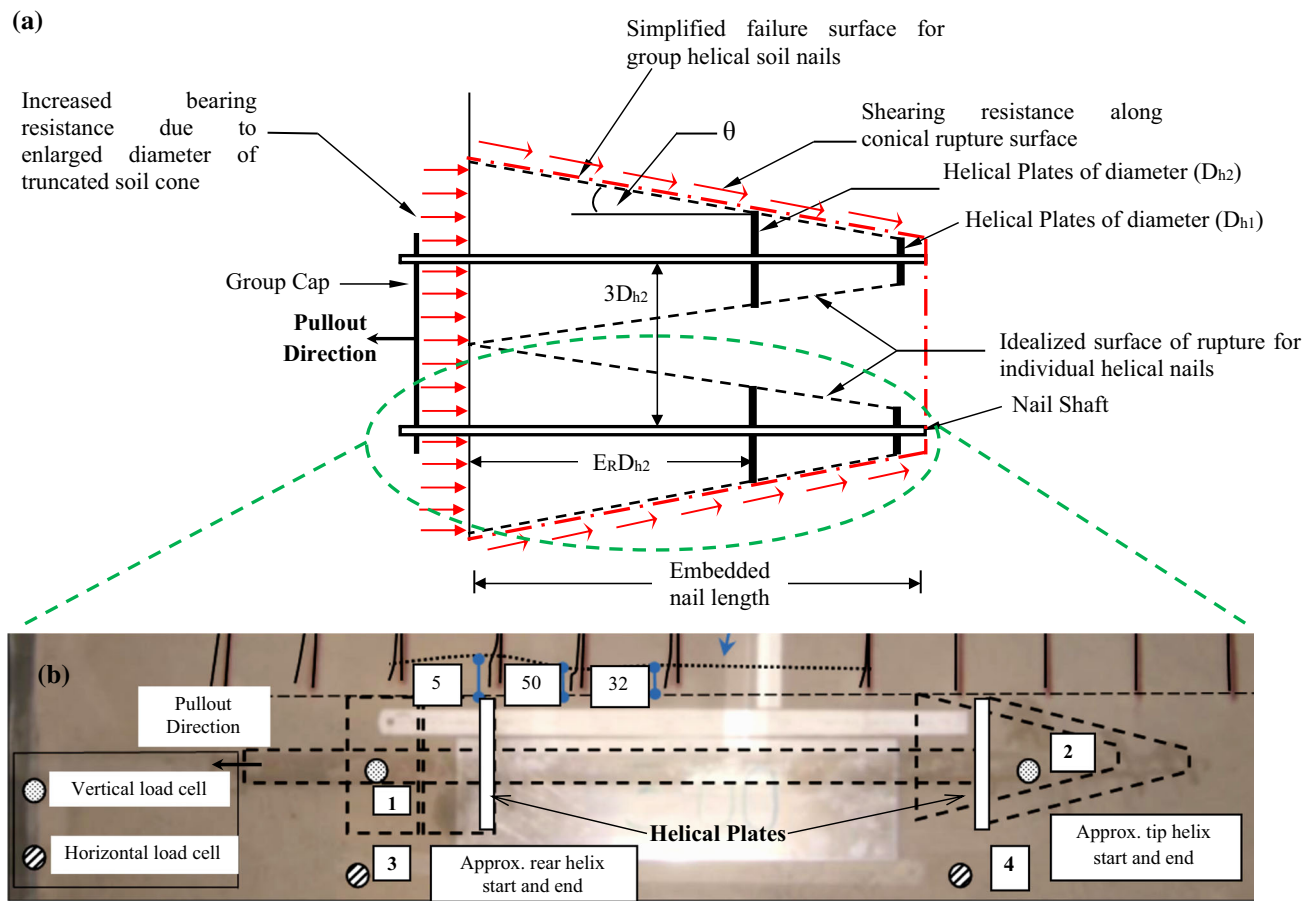
(a)

(b)

Fig. 1 Failure surface **a** group of helical soil nails simplified after Tokhi, 2016 **b** actual failure Tokhi, 2016 for single helical soil nail

governed by the shear resistance of the nail shaft and helical plate bearing resistance given by Eq. (1) modified in the present manuscript after Perko [10] as:

$$P_R = \pi d_s L_N \sigma_{avg} \tan \delta + \sum A_{Helix}\left(K_P \sigma_{avg} N_q\right) \tag{1}$$

In Eq. (1), average normal stress (σ_{avg}) is adopted to counter for both vertical (σ_v) and horizontal (σ_h) stresses acting on the circular surface area of the nail shaft. The average normal stress is calculated using Eq. (2) as:

$$\sigma_{avg} = \frac{\sigma_v + \sigma_h}{2} = \frac{\sigma_v(1 + K_0)}{2} = \frac{\sigma_v(2 - \sin \varphi)}{2} \tag{2}$$

In Eqs. (1) and (2), ds = diameter of helical nail shaft; L_N = length of helical nail behind the slip surface; δ = soil–nail interface frictional angle; A_{Helix} = surface area of the helix in contact with soil; and K_P = coefficient of passive earth pressure = $\frac{(1+ \sin\phi)}{(1- \sin\phi)}$.

Zhou [5] reported that redistribution of stresses around the drilled hole can be neglected when the installation procedure for grouted nails is not considered. Hence, the ratio of horizontal stress to vertical stress can be taken equal to the earth pressure at rest (K_0) condition. However,

in the present study, the torque installation of helical nails leads to transversing of soil and redistribution of stress around the helical plates as the nail installation progresses. Thus, to precisely account for the stress redistribution after nail installation, K_p represents a more realistic earth pressure situation around the helical nail. Likewise, during pullout, the helical plate presses against the soil in the direction of monotonic load depicting passive earth pressure condition (K_p). Simultaneously, the soil behind the helical plate undergoes a momentary detachment leading to active earth pressure conditions (K_a). Hence, to account for soil resistance during pullout, K_p has been employed in place of K_0, ϕ = angle of internal friction of soil; K_0 = coefficient of earth pressure at rest = (1 – sinϕ); and N_q = modified Meyerhof bearing capacity factors.

However, as per FSI [11], Meyerhof bearing factors are recommended to be modified for installation disturbance of the helical element. Similarly, Perko [10] also suggested a disturbance factor (λ_d) equal to 0.87 to account for disturbances during operational and installation procedures which affect the pullout capacity of helical elements. Hence, Eq. (1) can be modified as:

$$P'_R = P_R \lambda_d \tag{3}$$

For the group of helical soil nails, each nail acting in individual bearing leads to the formation of a cylindrical surface extending from the penetrating nail head and touching the outer edges of the helical plates. Thus, the resistance against pullout for the helical soil nail group depends upon the mobilized shear stress acting along this enlarged cylindrical surface (Fig. 1). For helical plates of equal diameter, the formation of a cylindrical surface is obvious; however, the transition of the surface from cylindrical to the conical (tapered) surface is observed for helical nails with increasing helix diameter. The bond stress acting is therefore mobilized along this conical failure surface.

Ideally, the conical failure surface is complex and can be mapped using log spiral lines, but for simplification, straight lines are considered in the present analysis. Figure 1 shows that in a group action, instead of individual bearing resistance through helical plates, bearing resistance is majorly dependent on the truncated cone that extends beyond the last helix. The bearing offered by the enlarged diameter can thus be given by taking into consideration the increased volume of soil within the truncated soil cone.

Simultaneously, shearing resistance is mobilized along the lateral surface of the enlarged conical rupture surface between the first and last helix. In the present case, the slanting surface of the conical failure zone is assumed to vary linearly between the first and last helix. Also, the shearing resistance acting along the first helix and penetrating nail head are neglected as the conical wedge formed has a significantly smaller surface area in comparison with the inter-helical rupture surface area. Figure 2 shows the sketch helical soil nail. Based on the assumptions and simplification, the pullout resistance for the helical soil nail group can be given by Eq. (4):

$$P_{\text{group}} = K_P \sigma_{\text{avg}} N_q C_N$$
$$+ \left[\pi(D_{c1} + D_{c2}) \sqrt{(D_{c2} - D_{c1})^2 + (E_R D_{c1})^2} \right] K_P \sigma_{\text{avg}} \tan \delta \tag{4}$$

where C_N = weight of the conical region formed governed by the embedment depth ratio (E_R) defined as the ratio of the depth of frustum (H) to the diameter of the formed soil truncated cone (D_{c2}); N = number of helical nails in the group; D_{C2} = larger diameter of the truncated soil cone ($3ND_{h2} + 2E_R D_{h2}\tan\theta$); and D_{C1} = smaller diameter of truncated soil cone ($3ND_{h2}$). C_N can be calculated by Eq. (5) as:

$$C_N = \frac{\pi}{4} \gamma D_{h2}^3 \left[9N^2 E_R + 6NE_R^2 \tan \theta + \frac{4}{3} E_R^3 \tan^2 \theta \right] \tag{5}$$

Testing Program

The testing of the pullout of helical soil nails was conducted using an apparatus capable of both installation and pullout. Generally, in deformation and stability analysis of helical soil the nailed slope is a boundary value problem when consolidation and creep effects are neglected. For solving such a three-dimensional problem, three equilibrium stress equations, six strain compatibility equations and six constitutive equations are required. Using appropriate boundary conditions, the unknown six stresses, six strains, and three displacements values can be evaluated. Thus, for analysis of helical soil-nailed structure, non-uniform stress conditions are prevalent along the entire length of the helical soil nail. As previously mentioned, helical nail length within the active zone develops shear stresses in direction of the soil movement whereas the pullout length of helical nail residing in the passive zone has shear stress acting against the nail movement. Thus, by modeling the pullout nail length only, uniform stress conditions are mobilized. This simplifies the investigation of

Fig. 2 Helical soil nail
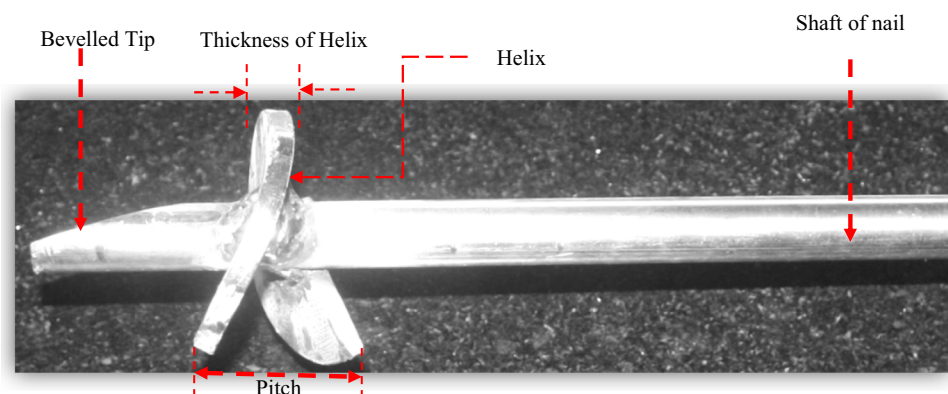
the effects of parameters such as overburden pressure, installation effects on stress–displacement, and the strength of helical nails during pullout [30].

In line with the stated reason, a model test tank of dimensions 2000 mm (long) × 1100 mm (wide) × 1100 mm (height) is used. The dimensioning of the tank is based on the finite element analysis carried out by Yin and Su [30] which suggested that stresses during drilling of 100 mm borehole reduce significantly at a lateral distance of 300 mm and vertical distance of 400 mm (about 1.9%). Moreover, Gurpersaud et al. [31] recommended that the minimum dimension for avoiding boundary effect be equal or greater than ten times the nail diameter. Since in the case of helical nails, the diameter of the helix governs the development of the influence zone, all dimensioning has been adopted according to the maximum helix diameter of size 96 mm. Thus, the minimum dimension for the model tank is adopted as 1100 mm > (10 × 96 mm) = 960 mm. The dimensioning has also been done to keep a clear edge distance of 2.5 D_h [32–35] for the case of the helical soil nail group.
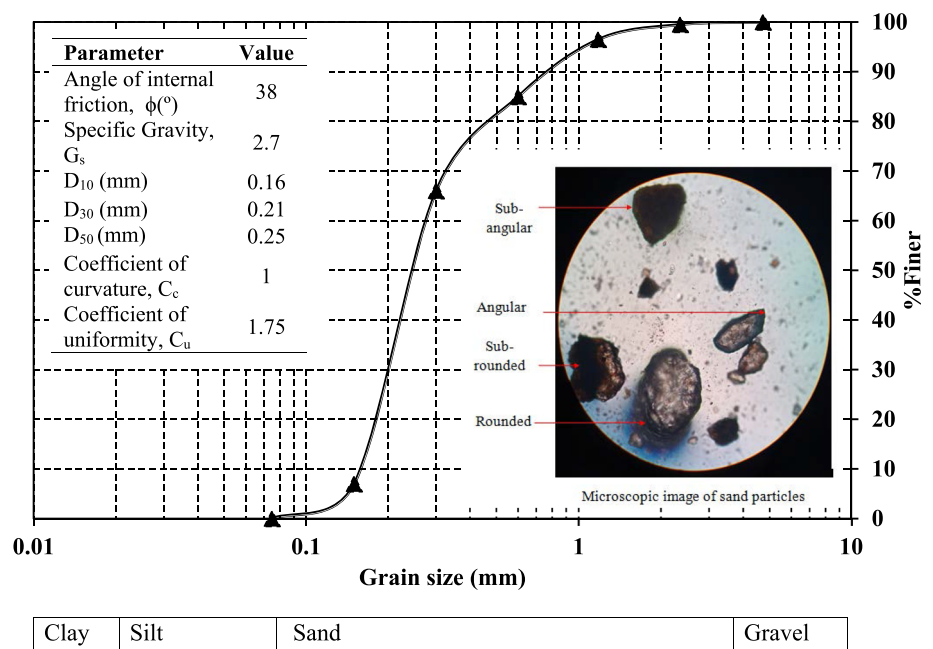
The model tank is filled with cohesionless soil classified as poorly graded sand having specific gravity (G) = 2.7; average grain size (D_{50}) = 0.25 mm; coefficient of uniformity (C_u) = 1.75; and coefficient of curvature (C_c) = 1. The angle of internal friction ($\phi°$) as determined from the direct shear test is 37.9° with an almost negligible cohesion (c) value taken as 0. All standard procedures of testing have been adopted as per IS codes [36] (Fig. 3). As per the field conditions, the relative density of soil is 80% to 90%

for soil nailing structures [1, 11] and is maintained at 86% for all the testing. The dry pluviation or the raining of sand is a commonly employed technique used to prepare sand samples in the laboratory to some specified initial state. The technique is calibrated so that the density of the samples produced is known accurately and precisely. The relative density of sand has been influenced by the size, gradation, and shape of the particle. The bigger size of particles leads to the greater kinetic energy of particles impacting the sand bed resulting in densified soil mass [37]. Thus, the relative densities from 30 to 100% are easily achievable using this technique without compaction. The sand fall heights greater than 0.5 m have no affected on density and are confirmed as reported by Okamoto and Fityus [38].

In the present study, the filling of the model tank is carried out by the pluviation technique by free-falling soil from a height of 108 cm with a constant check on relative density attained after every 200 mm filling. It was observed that the achieved relative density of the filled tank was about to 86 ± 2%, which is checked at different depths using the sand replacement method. A similar type of method has been suggested by Cresswell et al. [39] and Rad and Tumay [40] for the preparation of the sand sample.

For attaining the in situ equilibrium stress condition for the soil filled in the tank, a seating load of 2 kN is applied using a hydraulic jack. The hydraulic jack is fixed against a steel reaction frame designed for negligible deflection under reaction from a hydraulic jack. It is also ensured that

Fig. 3 Particle size distribution of soil used. Note: D_{50}, average grain size. D_{10}, D_{30}, and D_{60} are the soil grains diameter where 10%, 30%, and 60% of the particles are finer than this size, respectively

Parameter	Value
Angle of internal friction, $\phi(°)$	38
Specific Gravity, G_s	2.7
D_{10} (mm)	0.16
D_{30} (mm)	0.21
D_{50} (mm)	0.25
Coefficient of curvature, C_c	1
Coefficient of uniformity, C_u	1.75

no self-weight of the reaction frame accounts for the load applied over the soil tank. The seating load is kept for 24 h before the installation of the helical soil nail. Since helical soil nail structures are used as rectification measures, testing of pullout behavior under overburden pressure becomes necessary for keeping the study close to field conditions.

Therefore, four different overburden pressures of 5 kPa, 12.5 kPa, 25 kPa, and 50 kPa are used in the study. For testing of the pullout of traditional soil nails, an overburden range varying between 0 and 150 kPa has been employed by many researchers in the past [19, 21, 25]. As per Pradhan et al. [21], an overburden pressure of 150 kPa generally corresponds to an overburden caused by a fill having a height of 6–7 m. Since installation operations of nails were carried out with top to down construction approach, the lower range of overburden pressure (0–50 kPa) reflects a fill height of 2 m [1]. Secondly, an equipment limitation was also observed in the form of heating and oil spilling from hydraulic jack when overburden pressure beyond 50 kPa, as pressure was maintained for long durations. The hydraulic jack was connected with a load cell for recording the real-time load application. To ensure uniform load distribution from the hydraulic jack, a steel plate of thickness 10 mm was placed on the top of the soil surface. The plate thickness was initially checked for any deformation under sustained loading and thus adopted. The settlement of the top plate under loading is further recorded using LVDTs attached in a triangular arrangement around the loading plunger.

The helical soil nails used in field application generally have shaft diameters ranging between 38 and 88 mm. For helical soil nails to act in an individual bearing mechanism, the ratio of $D_h/d \geq 3$ is suggested by Hubbell [41]. Therefore, helical diameter ranging between 152 and 356 mm is traditionally employed. Similarly, with inter-helical spacing of $3D_h$ and the number of helical plates equal to 3, helical soil nail length is determined based on the ratio of the length of helical soil nail (L) to the height of the helical nailed wall (H). The suggested ratio lies between 0.7 and 1.2 as per FHWA [1]. For model helical anchors, Schiavon et al. [42] reported that the scale effects during model testing are governed by two parameters: (a) effect of mean particle size (D_{50}) on the shaft diameter (d) accounting for the shaft shearing resistance and (b) effect of mean particle size (D_{50}) on the wing ratio (W_R) accounting for the bearing resistance of the helical plates. The wing ratio (W_R) is defined as the difference of helix diameter to shaft diameter calculated as 0.5 ($D_h - d$). Thus, Schiavon, et al. [42] recommended that for avoiding scale effect on shaft shearing resistance $d/D_{50} > 30 - 50$ and $W_R/D_{50} > 58$ for no scale effect on helical bearing resistance.
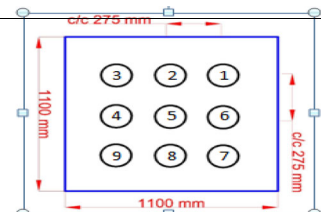
Moreover, Rotte and Viswanadham [43] employed a factor of 5, to scale down prototype soil nails to model soil nails. Hence, for the present study, a field helical shaft diameter of 80 mm is scaled down by 5, to adopt a shaft diameter of 16 mm. The length of the helical nail adopted for a height of 1000 mm with an L/H ratio of 0.9 is 900 mm for the present study. The nail length embedded in the soil tank used is 770 mm, and the remaining 130 mm is used for clamping purposes. To facilitate ease of penetration, the front 20 mm of helical nail penetrating head is beveled at an angle of 30° with the penetration axis. All the corresponding helical nail configuration details are summarized in Table 1.

The installation of helical nails both individual and group is attained by modifying the front panel of the model tank. The front iron panel was marked with a circular opening of a diameter slightly greater than 96 mm to accommodate the largest helix during installation and pullout. Likewise, for group helical soil nails, the uniform arrangement was formed by creating circular openings at the desired spacing of $3D_h$. For installation of the individual helical nail, the front panel is fixed at the model tank with a rubber membrane placed against the hole to prevent any soil from draining out during filling. Now, with the soil-filled tank and seated load placed for 24 h, the individual nail is installed at 20° with the horizontal. The angle of inclination for installation is adopted based on the fact that beyond 25°, compressive forces are mobilized which decreases the reinforcing action of nails [44].

The installation of helical nails is carried out by the pullout/torque installation machine which includes two three-phase induction motors (0.5 HP). The first motor allows forward and backward movement of the nail, while the second motor offers the revolution to the nail during installation. The device consists of a drive head for providing the necessary torque and rotation speed of 10–20 rpm display over-torque meter and RPM (revolutions per minute) gauge, respectively. The RPM gauge allows setting any rotation rate in the range of 10–20 rpm. The tail of the nail was gripped in the holding adaptor of the device, which revolves the nail at 10 rpm (adopted in the present study) and also provides a constant crowd force at a rate of penetration of one helix pitch in one revolution FSI [11]. The torque installation of the nail was carried up to a length of 700 mm with different nail inclination to the horizontal being achieved using the guided inclination arrangement of the apparatus [11, 41].

However, in the field practices, a standard backhoe attached with a torque head is used for helical soil nail installation. The helical soil nail length installed is about 700 mm out of the total 1000 mm used for nail fabrication. The remaining 300 mm is left to accommodate the clamping of nails in the adapters for installation and

Table 1 Details of individual and group of helical soil nails used in the study

Sr. No.	Nail Identification with shaft type	Shaft Diameter (d) (mm)		Helix Diameter, (D_h) (mm); $D_h > 3d$		Inter – helical spacing (s) $(s/D_h = 3)$		Pitch of helix (mm)		Number of Helices		Length of helical nail (mm) (Adopted $L/H = 0.9$)		For no scale effect d/D_{50}		W_R/D_{50}	
		Model	Prototype	Model	Prototype	Model	Prototype	Model	Prototype	Model	Prototype	Model	Prototype	Model	Prototype	Model	Prototype
Individual Helical soil nail																	
1	HSN (RS)	16	80	64 / 90 / 96	320 / 400 / 480	192 / 270 / 288	960 / 1200 / 1440	15	76	3	3	900	3650	64	> 30 – 50	160	>58
2	HSN (PH)	d_i 12 d_0 16	d_i 76 d_0 80	64 / 90 / 96	320 / 400 / 480	192 / 270 / 288	960 / 1200 / 1440	15	76	3	3	900	3650				
Helical soil nail Group																	

| Sr. No.		Spacing between Helical nails (mm) $(3D_h)$		No. of nails	Arrangement	Influence zone of each nail $(1.5D_h)$	Number of Helices	Clear edge distance (mm) $(>1.5\,D_h = 144)$	
		Vertical (S_V)	Horizontal (S_H)					From vertical edge	From horizontal edge
3	GHSN	275	275	9	Uniform	144	3	262	262

pullout. For the installation of a group of helical nails, the modified front panel (with nine circular openings) is attached in place. The top-down construction is adopted as per field practice with the top row of nails being installed first, one after the other, followed by the next row till all nine nails used in the group are installed. FSI [11] manual suggests the range of center to center spacing between helical elements (helical nails and helical tiebacks) from 1.5 D_h to 4.5 D_h (D_h = helical diameter), respectively, for no interference of adjacent element. In the present study due to the laboratory limit, the minimum spacing has been adopted 2.86 times bigger most helical diameter for group pullout. It is also observed by Mittal and Mukherjee [32–34] that the group behavior of helical anchors in sandy soil depicts no interference from the adjacent helical anchors for when helical anchors are spaced at 2.5 times the screw diameter. The rate of installation and penetration remains similar to the installation of the individual helical soil nail.

Prior to subjecting the nails to a pullout monotonic loading, installed nails are left undisturbed in the soil tank for one complete day (24 h) so that equilibrium in situ stress conditions are achieved. The pullout of individual/group nails is carried out by the same installation apparatus by moving it over a guided arrangement in the backward direction. During this maneuver, only translational backward movement is applied at a rate of 1 mm/min for simulating the monotonic pullout loading. The rate of the pullout is also determined based on the field pullout testing range of 1 mm/min (minimum) – 10 mm/min (maximum) as given by Hubbell [41]. The peak pullout force can be taken as either the maximum peak value or the point where increment in force per 1 mm displacement is less than 1% or a point where displacement reaches 30 mm [45].

In the present study, the pullout force is taken as the maximum peak value for both experimental and theoretical cases. The horizontal displacement (pullout length) is recorded using two LVDTs attached to the adapter, while the installation torque/pullout load is recorded by the torque meter and load cell attached within the 30-channel Universal Data Acquisition System (UDAS), respectively. Tensile testing (IS 1608:2005 [46]) on three specimens of hollow and rough nail shafts each was conducted using a UTM machine. The UTM was operated at a strain rate of 1 mm/min. for both ribbed solid and plain hollow nail. From the stress–strain plot for the hollow shaft section, the ratio of stress (within elastic limit) to the strain (i.e., E) was seen equal to 210GPa and 140GPa for ribbed solid and hollow shaft, respectively.

Fig. 4 Stress–displacement behavior of individual HSN under varying overburden pressure
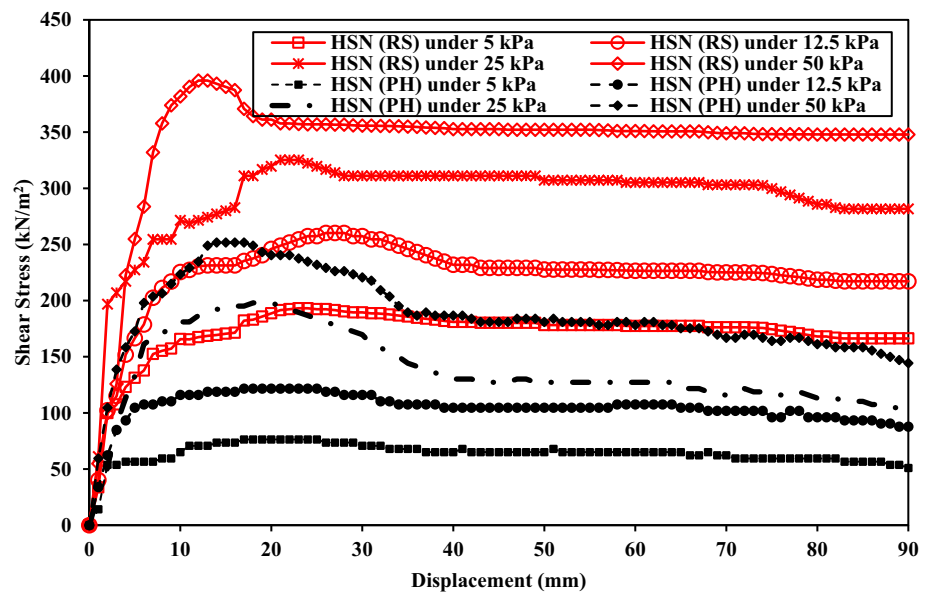
Results and Discussions

Stress–Displacement Behavior of Individual HSN

The stress–displacement behavior of individual HSN for both RS and PH at 20° with the horizontal is shown in Fig. 4. Figure 4 shows that the pre-peak and post-peak curve of shear stress with displacement under monotonic pullout loading follows a similar trend for both RS and PH helical nails. The mobilization of stress is found to increase with increasing displacement, till maximum shear stress is reached. With the further increment in displacement, mobilization of shear stress starts to decrease or becomes constant. The initial increase in shear stress can be accounted for by the bearing resistance and shearing resistance mobilization as the nail begins to move out under the pullout loading. As seen from the mechanism, the truncated cone provides an increased bearing ahead of the last helix and simultaneously larger shearing resistance is mobilized around the increased surface area of the conical failure surface.

The fading off from the peak shear stress is attributed to the permanent deformation of soil that occurs under the monotonic loading. As external pullout force is applied to the nail shaft, the soil undergoes permanent deformations. The soil deformations occur momentarily till shearing resistance mobilizes along the outer edge of the helical plate. However, it can be observed that maximum shear stress mobilized in the case of HSN (RS) is significantly higher than HSN (PH) under the same overburden pressure. Likewise, it is seen that shear stress for both HSN (RS and PH) increases with an increase in overburden pressure from 5 to 50 kPa. This is obvious as normal stress around the

HSN increases which increases the interface friction. However, it should be noted that as interface governing the mobilization of shearing resistance does not take place at the soil–HSN interface but at a larger radial distance away from the HSN shaft. Tokhi [25] also observe the pullout failure envelope of the helical nail and found that the rupture surface lies about 50 mm from helical plates, while 30 mm away from the nail shaft.

The low shear stress obtained for plain hollow helical nails as compared to rough solid helical nails has been accounted to the smaller resistance to nail displacement which occurs due to the tubular section of hollow nails. However, the authors agree that in addition to this, the surface roughness of plain and rough nails also contributes significantly to increasing the interface shearing resistance and hence yielding higher shear stress values for rough solid helical nails. The internal friction component helps only in installation and allows the soil to move into the pipe under compressive force up to the soil plugging stage. The plugged stage is the point where the soil does not move with respect to the inner wall of the hollow pipe. As the nail advance under compressive load, the plug densifies and the plug resistance builds up [12–14].

Thus, during pullout of the hollow nail, the contribution of effect of soil plugging in providing resistance against pullout is less significant as compared to the contribution of surface roughness of both the nail shafts (i.e., plain and rough). Additionally, for hollow and solid shafts with an equal amount of material, it is observed that hollow sections perform better than solid sections. However, in the present study, the hollow shafts used are three times lesser in weight than the solid nail with rough shaft rendering them with smaller pullout strength.

Fig. 5 a. Diagrammatic representation of location of strain gauges and earth pressure cells. **b**. Lateral stress around helical plates at different embedded length during peak shear stress
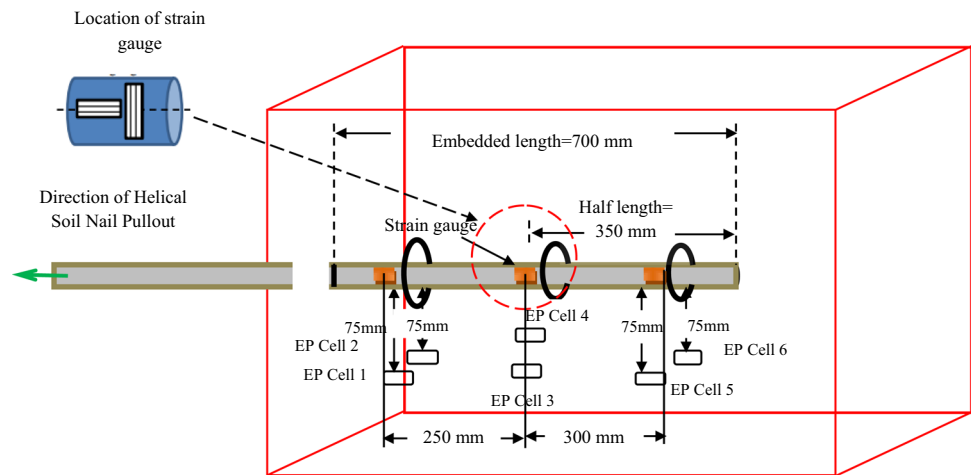
a Diagrammatic representation of location of strain gauges and earth pressure cells
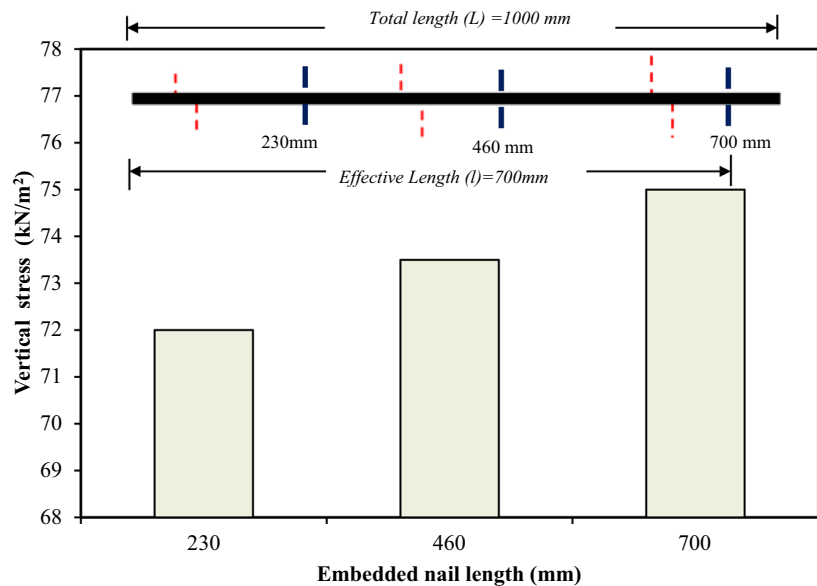
b Lateral stress around helical plates at different embedded length during peak shear stress

To further investigate the contribution of failure surface, vertical stresses around the helical plates are also recorded using earth pressure cells (Fig. 5a). The piezo-resistive type pressure transducers were used during laboratory testing. To investigate the vertical soil stresses around helical nails during pullout, six earth pressure cells of capacity 3 MPa were placed vertically below the nail. All six earth pressure cells were installed horizontally at depths of 70 mm above and below the nail length positioned 230 mm, 460 mm, and 700 mm away from the pullout nail end. Earth pressure cell was employed to record the real-time changing vertical stresses during installation and pull out of the soil nail. The pressure cells were calibrated over the whole operational range (0 to 50 kPa). The pressure was applied from 0 to 50 kPa using different weights,

while the response of increment in pressure was recorded from the data logger. The sensitivity of the earth pressure cell was recorded as 0.01 MPa.

As evident from Fig. 5b, vertical stress is found maximum around the first helical plates signifying increased bearing resistance to be overcome by the first helical plate under pullout loading. As the pullout length increases, the volume of soil in the conical rupture surface decreases, and hence smaller bearing is mobilized. Moreover, it can be deduced that confining pressure around the helical soil nail also increases with an increase in embedded nail length. The variation of vertical stress supports the criteria of development of non-uniform stresses around helical soil nails during monotonic pullout loading. Similar stress

conditions have also been found for traditional soil nails during pullout under surcharge loads [8, 30, 40].

Stress–Displacement Behavior of Group of HSN

Individual HSN was tested under different overburdens pressure of 5 kPa, 12.5 kPa, 25 kPa, and 50 kPa. As evident that with increases in surcharge pressures the pullout resistance of nail increases, but follow the same trend under different surcharge pressure. In order to investigate the group pullout capacity of a helical nail, testing conducted at 10 kPa lead to heating and misalignment of the pullout device significantly. In order to avoid inconsistent pullout values, group testing was conducted under an overburden pressure of less than 10 kPa. Hence, the qualitative comparison of individual and group HSN was reported at 5 kPa only. In addition, Junaideen et al. [19] and Pradhan et al. [21] reported that 7 m of wall height has equivalent pressure up to 150 kPa for pullout study of grouted nails. Thus, 5 kPa of overburden pressure can be accounted for fill height of 1–2 m, respectively.

A group of nine helical soil nails was investigated for stress–displacement behavior under monotonic pullout loading with an overburden pressure of 5 kPa. Abiding by the field practice, a uniform group arrangement has been adopted (Table 1). Figure 6 shows that stress–displacement behavior for the helical nail group follows a similar pattern as individual helical nails. The variation is marked by an initial elastic phase (pre-peak) as the maximum shear stress value is reached. Therefore, in the post-peak phase, a pure plastic behavior is depicted by the constant shear stress value under sustained displacement values. The increases in shear stress with initial pullout displacement can be contributed to the combined rupture surface formed. The individual helical nails are spaced at $3D_h$ distance such that

under pullout loading, the failure occurs against bearing and shearing from the combined failure surface in the form of a truncated cone. The maximum shear stress obtained using the helical soil nail group is approximately 425 kN/m^2 in comparison with HSN (RS) and HSN (PH) depicting maximum values of 190 kN/m^2 and 60 kN/m^2, respectively. Moreover, due to the enlarged failure surface and conical bearing, a significantly higher shear stress value is attained. The development of cumulative strain ($\frac{\Delta L}{L}$) around the single helical soil nails was found to be 14% more as compared to the strain developed during group pullout of the helical nail for similar nail arrangement.

Theoretical Analysis of Stress–Displacement Behavior of HSN

The theoretical modeling of shear stress–displacement behavior helps in estimating the long term performance of the helical soil-nailed structure. Moreover, validation of experimental results by theoretical results further helps in the rectification of discrepancy related to laboratory tests due to restrictions of accurate simulation. As discussed earlier in Fig. 4, the shear stress behavior of HSN (RS) and HSN (PH) under different surcharge pressure completely depends upon the pullout loading and corresponding nail displacement. Furthermore, Fig. 4 shows that the stress–displacement curve can be divided into two distinct stages, namely (a) pre-peak stage and (b) post-peak stage. The last value of pre-peak is equal to the first value of post-peak that is a common point for both cases. Hence, the last point of pre-peak and the first point of post-peak is the peak value.

Fig. 6 Stress–displacement behavior of group of 9 HSN (RS) with uniform spacing under 5 kPa
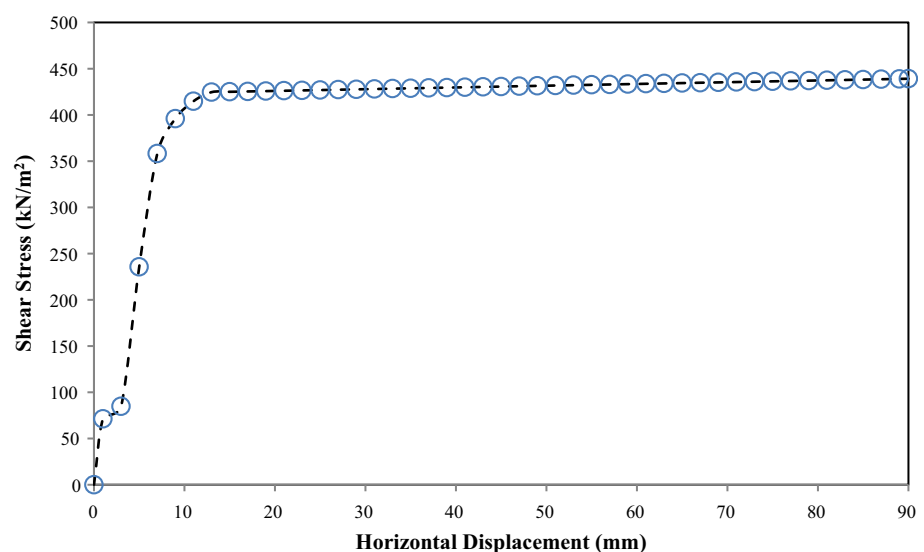
Analysis of Pre-Peak Stage

A helical nail is a tension member having a helical diameter (D_h), installation length (l), and modulus of elasticity (E). For an installed nail in soil pullout force (F) has been applied to the nail which produces tension in the soil nail and can be expressed as in Eq. (6). Equations (6) to (11) are exclusively for helical soil nails and not conventional nails. The models have been modified after (Kondner [47]; Zhang et al. [48]):

$$F(x) = \frac{\pi}{4} D_h^2 E \varepsilon(x) \tag{6}$$

where $F(x)$ = force applied on the soil nail at x distance from the nail head; $\varepsilon(x)$ is axial strain at point x, which is given as in Eq. (7):

$$\varepsilon(x) = \frac{\mathrm{d}u(x)}{\mathrm{d}x} \tag{7}$$

where $\mathrm{d}u(x)$ is a change in the position of the nail due to pullout force. Due to this resisting force (tension), mobilization of shear stress occurs between the interfaces. Consider force equilibrium of small section of nail dx in concurrence with the x-direction given as in Eq. (8):

$$\frac{\partial F(x)}{\partial x} = -\pi \cdot D_h \tau \cdot (x) \tag{8}$$

where τ is shear stress between the interface. Kondner [47] reported a nonlinear model for the pre-peak stage in shear stress ($\tau(x)$) versus pullout displacement $u(x)$ curve, expressed as in Eq. (9):

$$\tau(x) = \frac{u(x)}{\frac{1}{K} + \frac{u(x)}{\tau_{ult}}} \tag{9}$$

where $u(x)$ is the displacement during pullout; τ_{ult} is ultimate shear stress; and K is the slope of shear stress–displacement curve. The K value depends upon overburden pressure (σ) and can be represented from Eq. (10) developed from Fig. 7

$$K = 0.016\sigma - 0.07 \tag{10}$$

Using Eqs. (6)–(10), second-order differential equation has been generated [49] accounted with the variation of helical diameter for helical nail in Eq. (11):

$$\frac{\partial^2 F(x)}{\partial x^2} = \frac{4KF(x)}{\pi^2 E D_h^3 \tau_{ult}^2} \left[\frac{\mathrm{d}F(x)}{\mathrm{d}(x)} + \pi D_h \tau_{ult} \right]^2 \tag{11}$$

The second-order differential can be solved using appropriate boundary conditions. It is observed that since helical soil nails are treated as inextensible, all the force applied under monotonic pullout loading acts at the point of load application (i.e., helical nail toe). Similarly, shear stress dissipates after reaching a peak value and becomes negligible at the nail head. Hence, the following boundary condition is given in Eqs. (12) and (13) are applied as:

$$F(x = 0) = F_0 \tag{12}$$

$$F(x = L) = 0 \tag{13}$$

where L has installed length of the helical nail; and F_0 = Initial pullout load.

Equation (11) is the governing differential equation that presents the change in force with a displacement of the helical nail. The change in pullout load can be further used to estimate the mobilized shear stress with displacement using Eq. (8). The various parameter that is required to solve Eq. (11) are D_h, E, K, and τ_{ult}. As per design requirements, D_h is known, whereas the E and K can be estimated from experimental results. The ultimate shear strength (τ_{ult}) can be calculated as the ratio of peak shear strength (τ_p) to failure ratio factor (f_r), further which is the ratio of peak shear strength to ultimate shear stress [24]

Fig. 7 Variation of K with overburden pressure

$K = 0.016\sigma - 0.07$
$R^2 = 0.92$
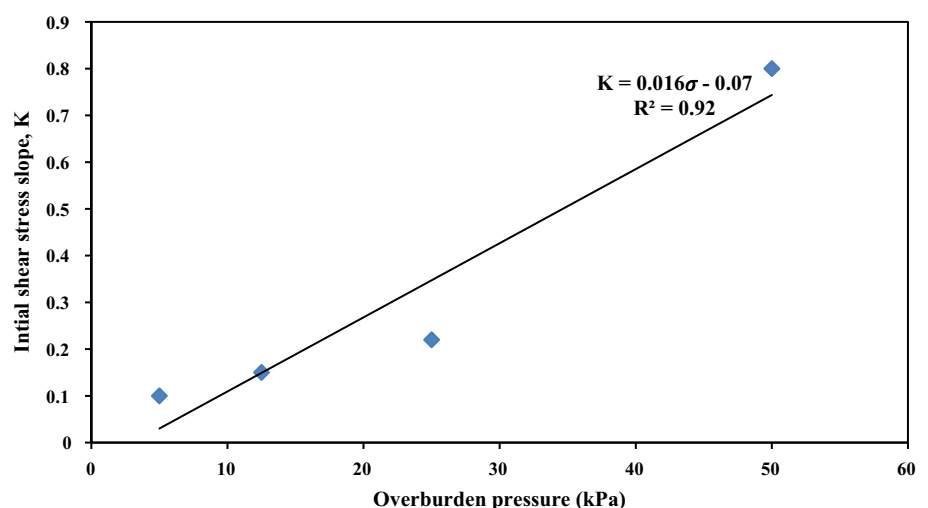
$$f_r = \frac{\tau_p}{\tau_{\text{ult}}} \qquad (14)$$

Analysis of Post-Peak Stage

To describe the post-peak stage of stress–displacement behavior of HSN, it is observed that beyond the peak value, shear stress begins to fade until a residual shear stress value is reached. To quantify this change from peak to residual, a residual factor (*f*) [24, 47] was calculated by Eq. (15) as:

$$f = \frac{\tau_p - \tau}{\tau_p - \tau_r} \qquad (15)$$

τ_p = peak shear strength between interfaces; τ_r = residual interface shear strength between interfaces; and τ = initial shear strength. The change in residual factor with displacement in the post-peak stage can be given by Eq. (16) as developed from Fig. 8.

$$f = 0.97ln[u(x)] - 3.12 \qquad (16)$$

where $u(x)$ = pullout shear displacement at post-elastic stage. Using Eqs. (15) and (16), the post-peak shear stress can be predicted. Combining Eq. (11) for pre-peak and Eq. (15) for post-peak, theoretical estimation of shear stress with displacement under varying overburden pressure can be made. As evident from Fig. 9, experimentally measured and theoretically simulated results for HSN shear stress–displacement are found in good agreement with a coefficient of variation (COV) ranging between 2 and 3 for 5 kPa, 12.5 kPa, and 25 kPa. However, a higher COV of 17 is attained for 50 kPa (Table 2).

Development of Axial Strains

The axial strains were measured using twelve strain gauges fixed at three different locations along the nail length. Strain gauges were placed parallel along the nail axis, while the other two perpendiculars to the nail axis [50].
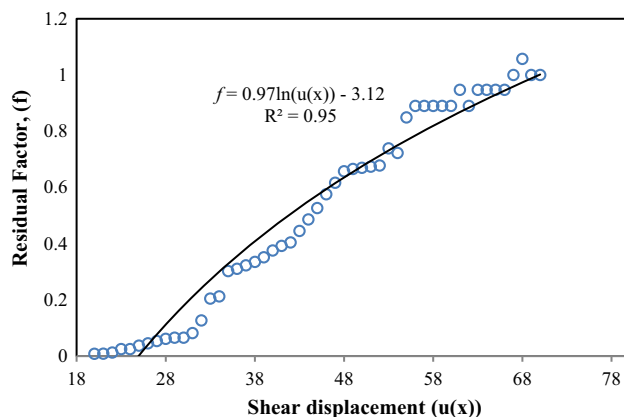

Fig. 8 Variation of residual factor with post-peak HSN displacement

This orientation of each set of two strain gauges was pasted near the head, tail, and center of the nail, respectively. To check the consistency of the strain result, six more strain gauges were pasted on the opposite side of the previously pasted gauges. The distance of each set from the head of the nail was 50 mm, 350 mm, and 600 mm, respectively. The detailed procedure of strain gauge installation has been elaborated in Sharma et al. [8].

Figure 10a, b shows that initially when horizontal displacement under pullout loading is small, a linear variation of axial strain is observed. This indicates that initially, the stress distribution along the nail is uniform. However, on further increase in nail displacement under monotonic loading, axial strain variation becomes nonlinear. The strains in HSN (PH) are significantly larger than the HSN (RS). On the basis of strain trend, the interface between soil and nail can be characterized into three typical zones. It includes the stress release state, the stress transferring state, and the part subjected to constant tension effect. When pullout force is applied over the nail due to tension deformation, the redistribution of stress or stress release along the nail will undergo. The second is the transition zone where the strain increase and further starts decreasing after attaining peak strain position. And the third zone is where the interface friction between soil and nail is still subjected to tension effect. It is during this tension effect stage that soil begins to depict the strain-softening effect. The zigzag pattern of axial strains with displacement for both HSNs (RS and PH) is due to the occurrence of strain softening in soil. For the group of HSN (Fig. 10c), it is observed that maximum axial strains are observed for nail numbers 5, 8, and 6, whereas nail numbers 1, 2, and 3 depicts low axial strain values.

Based on the observation, it can be stated that maximum axial strains are found along with nails that are under the direct influence of monotonic load application. It can also be deduced that top row of nails (i.e., 1, 2 and 3) undergo smaller horizontal pull as compared to the middle and last row of HSNs. Further, if the locus of maximum axial strain values along all 9 HSNs is traced, it will originate close to the tank surface for the last row of nails and further away for the top HSN row. This locus can be treated as a path for the occurrence of the slip failure surface. Based on the predicted slip surface, it may be recommended to opt for a smaller HSN length in the last rows and a larger HSN length in the upper rows. This result is in close accordance with the construction methodology recommended by FHWA [1]. However, one critical observation for group HSN is the non-formation of strain-softening effect. This could be explained based on the larger volume of soil restrained in the truncated cone formed during group failure.

Fig. 9 Measured
(experimental) and simulated
(theoretical) shear stress–
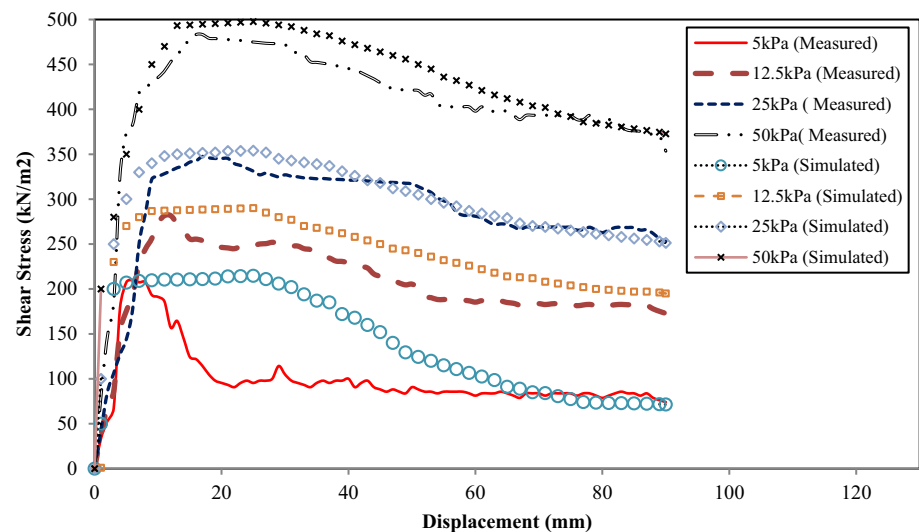displacement behavior of HSN
under varying overburden

Table 2 Statistical variation between measured and simulated results

Overburden pressure (kPa)	Measured peak shear stress HSN (RS) (kPa)	Simulated peak shear stress HSN (RS) (kPa)	Coefficient of variance (COV)
5	205.03	214.61	3.22
12.5 kPa	276.54	290.08	3.38
25 kPa	343.30	354.00	2.17
50 kPa	391.06	497.65	16.96

Conclusions

In this study, the pullout stress–displacement behavior of HSNs has been investigated under different overburden pressure and monotonic pullout loading. The experimental results are further validated by theoretical modeling of stress–displacement HSN behavior for pre-peak and post-peak stages. In addition, the vertical stresses and axial strain around HSN are also studied. Based on the experimental and theoretical results, the following conclusion can be drawn:

1. The stress–displacement behavior of HSN is nonlinear depicting an initial increase to reach a peak value, and then, gradually fading off until residual stress is reached. The trend of stress–displacement for both individual and group HSN is almost identical with more shear stress variation in the case of individual HSN for post-peak behavior. The stress–displacement behavior is governed by the truncated cone rupture surface formed during monotonic pullout loading. Further, based on shear stress behavior, HSN (RS) is found to perform better as compared to HSN (PH). It is also concluded that increased bearing obtained due to enlarged truncated cone failure surface contribute

significantly as compared to shearing resistance or resistance due to soil plugging as in the case of HSN (PH). This is further validated from the vertical stress variation along the HSN embedded length.

2. The experimentally measured results are in good agreement with the theoretical simulated result for pre-peak and post-peak shear strength stage under varying pressure for pullout helical soil nail with a small coefficient of variance of 2–3% for overburden pressure between 5 and 25 kPa. Hence, the developed theoretical model for HSN can be used to predict stress–displacement behavior for the overburden range up to 50 kPa. In addition, solid and hollow nails follow a similar trend for the pre-peak and post-peak shear strength stages.

3. The axial strain variation for both HSN (RS) and (PH) depicts the strain-softening effect. This strain softening is diminished as the number of HSN is increased in the case of group HSN. The variation of axial strain is more for HSN directly under the loading point as decreases for upper rows of nails. The construction methodology of using smaller length in the last rows and larger in the upper rows is also valid for HSN. This conclusion can be realized from the locus of maximum axial strain along HSN length.
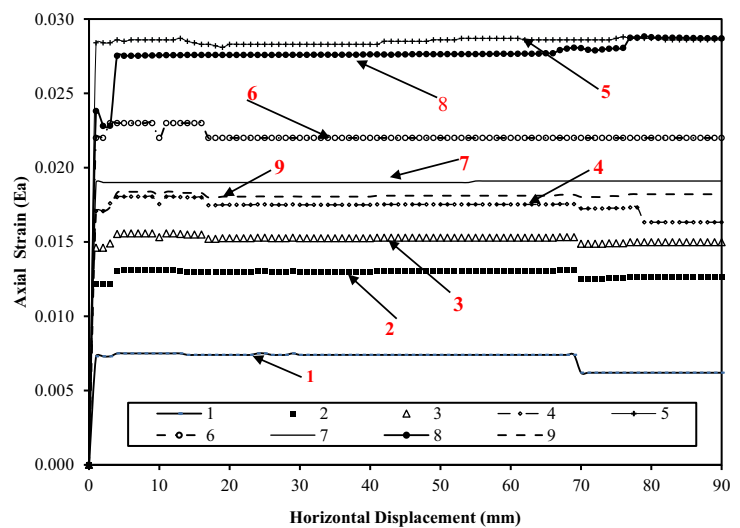
Fig. 10 a Variation of axial strain with pullout displacement under different surcharge pressure (solid shaft nail). **b** Variation of axial strain with pullout displacement under different surcharge pressure (hollow shaft nail). **c** Variation of axial strain with group pullout of nails having uniform spacing
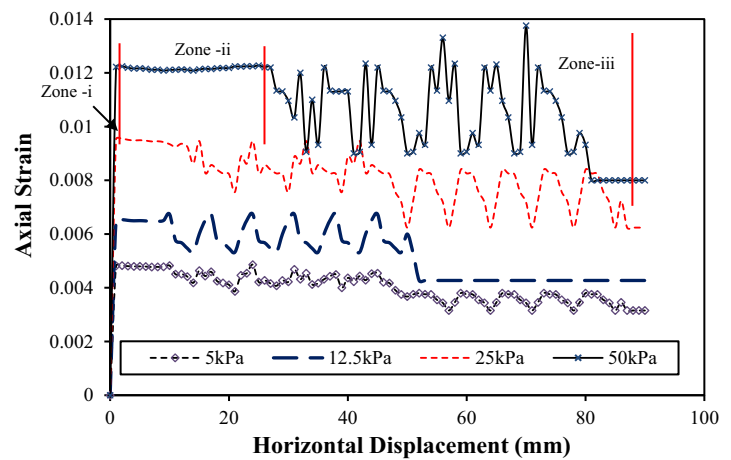
a Variation of Axial strain with pullout displacement under different surcharge pressure (solid shaft nail)
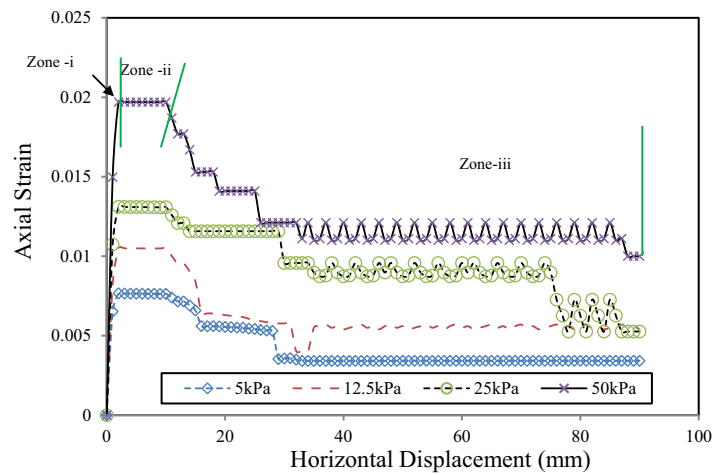
b Variation of Axial strain with pullout displacement under different surcharge pressure (hollow shaft nail)

c Variation of Axial strain with group pullout of nails having uniform spacing

Limitation of the Present Study

The effect of overburden on the conical failure rupture surface for both individual and group HSN is neglected in the present study. However, a thorough investigation is needed for accurately predicting the shape and nature of failure rupture surface with vertical overburden pressure in the case of HSNs. Due to the limited capacity of equipment, group analysis of HSN is conducted under low overburden pressure of 5 kPa only. Moreover, no vertical stresses are investigated during group HSN behavior under loading. Therefore, for predicting more realistic group behavior and corresponding confining stresses around the HSN group, studies with higher overburden pressure should be conducted. During the theoretical modeling, the soil dilation effect should be considered for higher ϕ values of soil. The above-mentioned investigation will significant contribute to a better comprehension of HSN behavior.

Availability of Data and Materials All the data used in the analysis is given in the manuscript. However, the authors will provide the data whenever required.

Code Availability Not applicable.

Compliance with Ethical Standards

Competing interests The authors declare that they have no conflict of interest.

References

1. FHWA (2015) Geotechnical engineering circular No. 7: Soil nail walls—reference manual. FHWA, Washington, D.C. Rep. No. FHWA-NHI-14–007.
2. Prashant A, Mousumi M (2010) Soil nailing for stabilization of steep slopes near railway tracks. Railway Design and Standard Organization (RDSO), Lucknow, India
3. Cheng YM and Wei WB (2007) Application of innovative GFRP pipe soil nail system in Hong Kong. doi:https://doi.org/10.4028/0-87849-456-1.3006
4. Dai ZH, Guo WD, Zheng GX, Ou Y, Chen YJ (2016) Moso bamboo soil-nailed wall and its 3D nonlinear numerical analysis. Int J Geomech doi: https://doi.org/10.1061/(ASCE)GM.1943-5622.0000634
5. Zhou W (2008) Experimental and theoretical study on pullout resistance of grouted soil nails (Doctoral dissertation, The Hong Kong Polytechnic University).
6. Sharma P, Rawat S, Gupta AK (2018) Study and remedy of kotropi landslide in Himachal Pradesh, India. Indian Geotechn J 48(4):1–17. https://doi.org/10.1007/s40098-018-0343-1
7. Rawat S, Gupta AK (2017) Numerical modelling of pullout of helical soil nail. J Rock Mech Geotechn Eng 9(4):648–658. https://doi.org/10.1016/j.jrmge.2017.01.007
8. Sharma P, Rawat S, Gupta AK (2020) Laboratory investigation of pullout behavior of hollow and solid shaft helical nail in frictional soil. Acta Geotech. https://doi.org/10.1007/s11440-020-01069-6
9. Mitsch MP and Clemence SP (1985) Uplift capacity of Helix anchors in sand.
10. Perko HA (2009) Helical piles: a practical guide to design and installation. Wiley, Hoboken
11. FSI (2014) Technical manual: helical piles and anchors, hydraulically driven push piers, polyurethane injection & supplemental support systems, 2nd edn. Foundation Support Works, Omaha, pp 33–39
12. Han F, Ganju E, Salgado R, Prezzi M (2019) Comparison of the load response of closed-ended and open-ended pipe piles driven in gravelly sand. Acta Geotech 14:1785–1803. https://doi.org/10.1007/s11440-019-00863-1
13. Sharma P, Rawat S, Gupta AK (2020) Horizontal pullout behavior of novel open-ended pipe helical soil nail in frictional soil. Int J Civ Eng. doi:https://doi.org/10.1007/s40999-020-00535-2
14. Sharma P, Rawat S, Gupta AK (2021) Laboratory investigation of pullout behavior of open-ended pipe helical soil nail in frictional soil. Geotech Geol Eng. https://doi.org/10.1007/s10706-020-01666-y
15. Singh K, Mittal S, Kumar K (2018) Reduction in lateral displacement of cohesionless soil at box tunnel face using nails in overburden. Int J Geosynthetics Ground Eng 4(21). https://doi.org/https://doi.org/10.1007/s40891-018-0138-6
16. Su LJ, Chan TCF, Yin JH, Shiu HYK, Chiu SL (2008) Influence of overburden pressure on soil nails pull-out resistance in a compacted fill. J Geotech Geoenviron Eng 134(9):1339–1347. https://doi.org/10.1061/(ASCE)1090-0241(2008)134:9(1339)
17. Hong CY, Liu ZX, Zhang YF, Zhang MX, Borana L (2007) Influence of critical parameters on the peak pullout resistance of soil nails under different testing conditions. Int J Geosynth Gr Eng. doi:https://doi.org/10.1007/s40891-017-0095-5
18. Hong CY, Yin JH, Zhou WH, Pei HF (2012) Analytical study on progressive pullout behavior of a soil nail. J Geotech Geoenviron Eng 138(4):500–507. https://doi.org/10.1061/(ASCE)GT.1943-5606.0000610
19. Junaideen SM, Tham LG, Law KT, Lee CF, Yue ZQ (2004) Laboratory study of soil–nail interaction in loose, completely decomposed granite. Can Geotech J 41(2):274–286. https://doi.org/https://doi.org/10.1139/t03-094
20. Chu LM, Yin JH (2005) Comparison of interface shear strength of soil nails measured by both direct shear box tests and pullout tests. J Geotechn Geo-environ Eng 131:1097–1107. https://doi.org/10.1061/(ASCE)1090-0241(2005)131:9(1097)
21. Pradhan B, Tham LG, Yue ZQ, Junaideen SM, Lee CF (2006) Soil-nail pullout interaction in loose fill materials. Int J Geomech 6(4):238–247. https://doi.org/10.1061/(ASCE)1532-3641(2006)6:4(238)
22. Hong CY, Yin JH, Pei HF, Zhou WH (2013) Experimental study on the pullout resistance of pressure-grouted soil nails in the field. Can Geotech J. doi:https://doi.org/10.1139/cgj-2012-0103
23. Sharma M, Samanta M, Sarkar S (2017) A laboratory study on pullout capacity of helical soil nail in cohesionless soil. Can Geotech J 54(10):1482–1495. https://doi.org/10.1139/cgj-2016-0243
24. Sharma M, Samanta M, Punetha P (2019) Experimental investigation and modeling of pullout response of soil nails in cohesionless medium. Int J Geomech ASCE 19(3):04019002-1-04019002-16. doi: https://doi.org/10.1061/(ASCE)GM.1943-5622.0001372.
25. Tokhi H (2016) A study of new screw soil nail. Dissertation, RMIT University, Melbourne

26. Sharma M, Samanta M, Sarkar S (2018) Novel laboratory pullout device for conventional and helical soil nails. Geotech Test J (ASTM) 42(5):1–23. https://doi.org/https://doi.org/10.1520/GTJ20170319

27. Rawat S, Gupta AK, Kumar A (2017) Pullout of soil nail with circular discs: a three-dimensional finite element analysis. J Rock Mech Geotech Eng 9:967–980. https://doi.org/10.1016/j.jrmge.2017.05.003

28. Rawat S, Gupta AK (2017) Testing and modeling of screw nailed soil slopes. Indian Geotech J 48(1):52–71. https://doi.org/10.1007/s40098-017-0229-7

29. Rawat S (2017) Testing and modeling of soil nailed slopes," Jaypee University of Information Technology, waknaghat, Solan, India

30. Yin JH, Su LJ (2006) An innovative laboratory box for testing nail pull-out resistance in soil. Geotech Test J 29(6):451–461. https://doi.org/10.1520/GTJ100216

31. Gurpersaud N, Vanapalli SK, Sivathayalan S (2013) Semi-empirical method for estimation of pull-out capacity of grouted soil nails in saturated and unsaturated soil environments. J Geotech Geo-environ Eng (ASCE) 139(11):1934–1943. https://doi.org/https://doi.org/10.1061/(ASCE)GT.1943-5606.0000883

32. Mittal S and Mukherjee S (2015) Behaviour of group of helical screw anchors under compressive loads. Geotech. Geol. Eng.,33,575–592.https://doi.org/https://doi.org/10.1007/s10706-015-9841-4

33. Mittal S, Mukherjee S (2013) Vertical uplift capacity of a group of helical screw anchors in sand. Indian Geotech J 43(3):238–250. https://doi.org/10.1007/s40098-013-0055-5

34. Mittal S, Mukherjee S (2014) Vertical pullout capacity of a group of helical screw anchors in sand: an empirical approach. Indian Geotech J 44(4):480–488. https://doi.org/10.1007/s40098-014-0099-1

35. Singh K, Mittal S, Kumar K (2019) Vertical displacement reduction of cohesionless overburden soil by nails in box jacking. Int J Geotech Eng 14(7):766–778. https://doi.org/10.1080/19386362.2019.1643521

36. IS: 2720-4 (1985) Grain size analysis. Bureau of Indian Standard (BIS), New Delhi

37. Vaid YP, Negussey D (1984) Relative density of pluviated sand samples. Soils Found 24(2):101–105

38. Okamoto M, Fityus S (2006) An evaluation of the dry pluviation preparation technique applied to silica sand samples. 1st Edition

39. Cresswell A, Barton ME, Brown R (1999) Determining the maximum density of sands by pluviation. Geotech Test J 22(4):324–328

40. Rad NS, Tumay MT (1987) Factors affecting sand specimen preparation by raining. Geotech Test J 10(1):31–37

41. Hubbell Power Systems (2015) Screw nailing retention earth structures, design manual. Chance. USA

42. Schiavon JA, Tsuha C, Thorel L (2016) Scale effect in centrifuge tests of helical anchors in sand. Int J Phys Modell Geotechn 16(4):185–196. https://doi.org/10.1680/jphmg.15.00047

43. Rotte VM, Viswanadham BVS (2013) Influence of nail inclination and facing material type on soil-nailed slopes. Proc ICE Ground Improve 166(2):86–107. https://doi.org/10.1680/grim.11.00026

44. Shiu YK, Chang GWK (2006) Effects of inclination, length pattern and bending stiffness of soil nails on behaviour of nailed structures, GEO Report No. 197 [Online]. Available: https://www.cedd.gov.hk/eng/publications/geo/geo-reports/geo_rpt197/index.html.

45. Zhang LL, Zhang LM, Tang WH (2009) Uncertainty of field pullout resistance of soil nails. J Geotech Geo-environ Eng 135(7):966–972. https://doi.org/10.1061/(ASCE)GT.1943-5606.0000014

46. Indian Standard Code (2005) Metallic materials-tensile testing at ambient temperature Third Revision. BIS

47. Kondner RL (1963) Hyperbolic stress-strain response: cohesive soils. J Soil Mech Found Div 89(1):115–143

48. Zhang CC, Xu Q, Zhu HH, Shi B, Yin JH (2014) Evaluations of load-deformation behavior of soil nail using hyperbolic pullout model. Geomech Eng 6(3): 277–292. https://doi.org/https://doi.org/10.12989/gae.2014.6.3.277.

49. Anubhav, Basudhar PK (2010) Modeling of soil-woven geotextile interface behavior from direct shear test results. Geotext Geomembranes. doi:https://doi.org/10.1016/j.geotexmem.2009.12.005

50. Omega.co.uk Positioning strain gages to monitor bending, axial, shear, and torsional loads: A guide to installation (E56). https://www.omega.co.uk/techref/pdf/Strain-gauge-application-info/how-to-position-strain-gauges.pdf Accessed on 2019